Applied Thermal Engineering 200 (2022) 117619

Contents lists available at ScienceDirect

Applied Thermal Engineering

journal homepage: www.elsevier.com/locate/ate

Research paper

Experimental development of a novel thermoelectric generator without moving parts to harness shallow hot dry rock fields

Patricia Alegria, Leyre Catalan, Miguel Araiz, Antonio Rodriguez, David Astrain *

Department of Engineering, Institute of Smart Cities, Public University of Navarre, Pamplona, Spain

ARTICLE INFO

Keywords:
Thermoelectric generator
Heat pipe
Thermosiphon
Fins dissipator
Thermoelectricity

ABSTRACT

Nowadays, geothermal energy in shallow hot dry rock fields is not exploited enough due to the high economic and environmental impact as well as the lack of scalability of the existing technologies. Here, thermoelectricity has a great future potential due to its robustness, absence of moving parts and modularity. However, the efficiency of a thermoelectric generator depends highly on the heat exchangers. In this work, a novel geothermal thermoelectric generator is experimentally developed, characterizing different configurations of biphasic heat exchangers to obtain low thermal resistances that allow the maximum efficiency in the thermoelectric modules. As a result, robust and passive heat exchangers were obtained with thermal resistances of 0.07 K/W and 0.4 K/W in the hot and cold sides, respectively. The geothermal thermoelectric generator was built with the most effective heat exchangers and was experimented under different temperature and convection conditions, generating 36 W (17 W by a prototype with 10 modules and 19 W by a prototype with 6 modules) for a temperature difference of 160 °C between the heat source and the environment. Furthermore, the experimental development showed that it is possible to increase electricity generation with a more compact generator, since a decrease in the number of modules from 10 to 6 increases the efficiency from 3.72% to 4.06%. With this research, the feasibility of a novel and robust geothermal thermoelectric generator whose working principle is phase change has been experimentally demonstrated, as well as the importance of compactness to maximize its efficiency and thus, power generation.

1. Introduction

The relentless increase in global energy demand and the over-development of fossil resources have led during the last century to a climate crisis. In this context, a transition from fossil fuels to renewable sources is highly needed. This is why most countries are making efforts to promote renewable energies, in order not to overpass the 1.5 °C target of Paris Agreement [1]. In recent years, hydro, wind and solar power have become the most popular ones due to their technological development, inducing a decrease in their prices. The problem is that these sources depend on the weather and they are not continuous. Geothermal energy has the advantage of a great stability producing non-stop energy, but this renewable source has been left behind the others in terms of growth rate and installed capacity due to the high initial investment, long payback time and construction time, difficulty to assess resource and to modularize [2]. It is estimated that if only 1% of geothermal heat available in the Earth's crust could be used, it would provide all the energy that the planet requires for 2800 years at a constant consumption rate [3]. Against this backdrop, it is important to bolster technology and harness the geothermal potential that exists in many regions. This will help to achieve the Sustainable Development Goals, specifically number 7 "Ensure access to affordable, reliable, sustainable and modern energy for all" and 11 "Make cities and human settlements inclusive, safe, resilient and sustainable", which were adopted by all United Nations Member States in 2015 to provide a shared blueprint for peace and prosperity for people and the planet before 2030 [4].

Geothermal energy can be used directly as heat and indirectly when it is converted into electricity. There are different geothermal resources depending on their temperature, and the type determines their utilization method. Low enthalpy resources (<100 °C) are used for heating, while electricity is generated with medium (100–150 °C) and high (>150 °C) enthalpy resources.

Nowadays, to obtain electric power from geothermal heat it is necessary a geothermal plant working with a thermodynamic cycle. Geothermal conventional power plants are similar to steam power plants, but they use Earth as a natural boiler [5]. In these systems, Earth's heat produces steam that, by expanding through a turbine, will excite a generator with a rotative movement, generating electricity.

* Corresponding author.
E-mail address: david.astrain@unavarra.es (D. Astrain).

https://doi.org/10.1016/j.applthermaleng.2021.117619
Received 24 May 2021; Received in revised form 9 September 2021; Accepted 22 September 2021
Available online 26 October 2021

Nomenclature

Variables

ΔT	Temperature difference (°C)
$\dot{Q}$	Heat flux (W)
η	Efficiency
η_{fins}	Fins' efficiency
A	Area (m^2)
h	Heat transfer coefficient (W/m^2K)
I	Intensity (A)
k	Thermal conductivity (W/mK)
m	Number of thermoelectric modules in a GTEG
P	Electric power (W)
R	Thermal resistance (K/W)
R_{Load}	Load electrical resistance (Ω)
T	Temperature (°C)
V	Voltage (V)
v	Velocity (m/s)

Subscripts and Superscripts

amb	Ambient
b	Boiling
C	Cold side of the thermoelectric module
c	Condenser/Condensation
$cond$	Conductive
$conv$	Convective
g	Ground
H	Hot side of the thermoelectric module
hp	Heat pipe
los	Losses
mod	Module
tot	Total

Abbreviations

[CHE]	Cold side Heat Exchanger
EGS	Enhanced Geothermal System
F	Forced convection
GTEG	Geothermal Thermoelectric Generator
HDR	Hot Dry Rock Field
HHE	Hot side Heat Exchanger
N	Natural convection
TEG	Thermoelectric Generator
TEM	Thermoelectric Module
TIM	Thermal Interface Material
TPCT	Two Phase Closed Thermosiphon

This technology always requires a geothermal system, which basically consists of a heat source, a carrier fluid and a reservoir.

High enthalpy reservoirs use the steam extracted from the resource, either directly (dry steam plants) or after a separation process in case there is water in the mixture (flash plants). The expanded steam is usually condensed for re-injection into the geothermal reservoir, creating a Rankine cycle. However, it sometimes happens that the degree of salinity is too high or that the temperature range is not sufficient. In such cases, the extracted mixture heats a secondary fluid that performs the cycle. These cycles are known as binary cycles. The secondary fluid can be water (conventional Rankine cycle) or other fluids that have low boiling points and high vapor pressures at low temperatures [6] (organic Rankine cycles or Kalina cycles) [7].

Among the high enthalpy geothermal resources, there is one, called hot dry rock field (HDR), which consists of hot impermeable rocks. Thus, these fields have naturally a heat source but not a fluid nor a reservoir. HDR represents over 99% of the total U.S. geothermal resource [8]. By the moment, there exists only one way to exploid this kind of geothermal field, in which boreholes are drilled and water is artificially injected into hot igneous rock that is heated by a process similar to the hydrothermal system [9], originating a man-made reservoir of several kilometers deep. This method, called Enhanced Geothermal System (EGS), may induce seismicities and entails a high economic expense and a high environmental impact. Moreover, the actual HDR turbine-based plants, do not permit scalability and that makes it difficult to operate at low power, they are only viable for high power. In this work, a novel technology is proposed to take advantage of shallow hot dry rock fields causing less impact and solving the mentioned problems: a geothermal thermoelectric generator (GTEG). It has been specifically developed for its future application in the shallow geothermal anomalies of Timanfaya National Park (Spain), where temperatures of 100–400 °C can be found at 1 m deep inside the ground [10,11].

A geothermal thermoelectric generator is a solid-state device that directly transforms thermal energy from the superficial Earth's crust into usable electricity. It contains three principal parts: The hot side heat exchanger (HHE), the thermoelectric module (TEM) and the cold side heat exchanger (CHE). The hot side heat exchanger transports the heat from a heat source (the geothermal source) to the hot side of the TEM. The thermoelectric module is the most important part, which is responsible of transforming part of the heat into electricity thanks to the Seebeck effect. The heat that is not transformed into electric energy must be dissipated into the cold source, usually the environment, for which a CHE is used. The module's efficiency highly depends on the temperature difference between its hot and cold sides [12]. These temperatures respectively depend on the ones of the heat and cold sources and on the thermal resistance of the heat exchangers, in the way that the lower their thermal resistances, the more similar the temperatures of the source and the module's face. This solution involves numerous advantages: robustness, modularizing capacity, no moving parts, no maintenance requirements, noiseless and minimal environmental impact.

Different thermoelectric generators (TEG) for geothermal energy can be found in the literature. Most are computational studies and few experimental, and what is more, in order to apply thermoelectric generation to geothermal energy, all of them use moving parts to circulate a fluid [13], thus losing the intrinsic advantage of thermoelectricity: the absence of moving parts.

Some researchers' aim is to increase the efficiency of conventional cycles such as Rankine or Kalina by introducing thermoelectricity [14]. By way of example, Khanmohammadi et al. [15], Gholamian et al. [16], and Malik et al. [17] propose TEGs for waste heat recovery in geothermal plants to increase the plant's output power.

Other authors are focused only on thermoelectric generators (TEGs) without conventional cycles. Sutter et al. modeled and optimized a 1 kWe thermoelectric stack for geothermal heat conversion with hot water inlet and outlet temperatures of 140 °C and 20 °C [18]. Liu et al. experimented in the laboratory a thermoelectric generator to use geothermal low-temperature heat, proposing a heat transmission by means of fluid from the geothermal source to the thermoelectric modules. They first esteemed (using experimental data) a generation of about 500 W with a temperature difference of about 200 °C between the hot and the cold side. Then, they developed a generator of 1 kW that worked with a temperature difference of around 120 °C using 600 TEMs. Their last experiment was a five-layer TEG which reached to generate 45.7 W with a ΔT of 72.2 °C between the hot and cold sides, in order to modularize for large-scale energy production [19–21].

Wang and Wu investigated a method to enrich the geothermal power generation in horizontal wells by attaching thermoelectric generators (TEG) to the outer surface of the tubing. With their simulation model, they obtained a total output power of 128 W [22]. Dell et al. developed a thermoelectric generator that can produce more than 5 W in steady-state in an environment which has a difference of 130 °C between the ambient air temperature and the surface of a geothermal steam pipe in Iceland [23]. Also for low geothermal temperatures, a portable thermoelectric generator was designed and experimented by Ahiska and Mamur, obtaining a maximum power of 41.6 W when the temperature difference between the surfaces of the TEG was 67 °C [24].

All the examples mentioned above use fluid as a heat carrier, which entails the use of pumps. Moreover, none of them is designed for high temperature geothermal fields. The only thermoelectric generator proposed to take advantage of the high enthalpy geothermal anomalies in hot dry rock fields is the one designed, computationally studied and validated by Catalan et al. [25]. It consists of biphasic thermosiphons with water as working fluid in both sides of the thermoelectric modules. This way, the solution has the advantage that it does not need water pumping, so it does not produce noise and it does not need maintenance nor auxiliary consumption. In their paper, a computational study is developed to model the GTEG's possibilities in a real location: Timanfaya National Park (Canary Islands, Spain), which is one of the greatest shallow HDR fields in the world [26,27]. They simulated the GTEG's behavior under different conditions and they computationally demonstrated the importance of using heat exchangers with low thermal resistance in order to maximize power generation [25].

As laboratory work should be done, this research deepens in the experimental operation of a geothermal thermoelectric generator based in biphasic passive heat exchangers, with the objective of obtaining the maximum power generation and optimizing the occupied space. Hence an experimental study of this technology is carried out, comparing the number of modules, different geometries of the cold side heat exchanger and different hot side thermosiphon heights in order to achieve robustness and compactness by using exchangers without moving parts and with low thermal resistances that allow maximizing the generation.

In Section 2, the heat exchangers are experimentally studied to select the best option for both the hot and cold sides. Section 3 describes the geothermal thermoelectric generator from the design to the final assembly. In Section 4, the results of the GTEG's experimentation are collected and finally, Section 5 contains the conclusions of the work.

2. Characterization of the heat exchangers

This geothermal thermoelectric generator works as Fig. 1 depicts. A two phase closed thermosiphon is inserted into the ground in a shallow hot dry rock field. As it absorbs the geothermal heat, the water inside boils and ascends to the upper part, where thermoelectric modules are located on the external surface. Here, the water inside condenses, transferring its latent heat of condensation to the modules. These modules directly transform part of the heat into electricity and the rest is dissipated to the environment by the cold side heat exchangers, which consist of aluminum fins dissipater with heat pipes, whose working principle is also phase change [25].

According to the thermal equivalent circuit of the GTEG represented in Fig. 1, the thermal resistances of the different parts of the GTEG have been studied. The heat flux extracted from the geothermal ground follows Eq. (1), where P is the electric power generated by each module, $\dot{Q}_C$ is the heat flux through the cold side heat exchangers and m the number of thermoelectric modules installed. The thermal resistance of the hot side heat exchanger (the two phase closed thermosiphon) R_{HHE} corresponds to Eq. (2), which is obtained by dividing the temperature gradient between the temperature of the ground and the one of the modules' hot side, by the heat flux extracted. In the same way, the cold side heat exchanger's thermal resistance R_{CHE} is obtained by dividing the temperature gradient between the modules' cold side and the environment, by the heat flux through it (Eq. (3)). Finally, the total thermal resistance of the GTEG can be obtained by Eq. (4).

$$\dot{Q}_H = Pm - \dot{Q}_C m \tag{1}$$

$$R_{HHE} = \frac{T_g - T_H}{\dot{Q}_H} \tag{2}$$

$$R_{CHE} = \frac{T_C - T_{amb}}{\dot{Q}_C} \tag{3}$$

$$R_{tot} = R_{HHE} + \frac{R_{mod}}{m} + \frac{R_{CHE}}{m} \tag{4}$$

If the heat exchangers' resistances are improved, the temperatures of the hot and cold sides of the module will be closer, respectively, to those of the hot and cold sources, so the TEMs efficiency will increase. This brings also another benefit: we will be able to extract a higher heat flow from the hot source. By passing a higher heat flux through the modules, the electrical power output is maximized.

As the heat exchangers are crucial for the operation of the GTEG, it is important to perform a deep analysis of their behavior separately. The experimental study of the heat exchangers had two objectives.

On the one hand, the objective for the hot side heat exchanger (TPCT) was to test for the first time that a thermosiphon of 3 m long is capable of transmitting the heat without big temperature losses from the hot source to the part where TEMs will be located. It is of interest to study how it works in different levels of the surface because TPCT's necessary length depends on the number of thermoelectric modules. The analysis will determine how this affects heat transportation. It is expected that, according to Eq. (4), if the modules number is increased, the efficiency and output power per TEM will decrease because the hot side thermal resistance per thermoelectric module is increased and that would lead to a decrease in T_H.

On the other hand, the second objective was to select the geometry and disposition of the cold side heat exchangers. These must have low thermal resistance in order to transport a heat flux that allows the modules to work with higher efficiency and more heat-to-electricity transformation. The lower their thermal resistance is, the higher the heat flux the cold side heat exchanger is able to transport.

The design of both exchangers should ensure a compact GTEG, which does not have a major environmental impact and which is also able to take advantage of the wind, an important factor for these totally passive heat exchangers to improve the convection coefficient, thus reducing their thermal resistance and increasing the power generated by the modules.

2.1. Hot side heat exchanger

The developed hot side heat exchanger of the GTEG is a two phase closed thermosiphon made of a 3 m copper tube with a diameter of 41.27 mm. These dimensions are based on previous computational studies of Catalan et al. [25]. It is responsible for transporting heat from the heat source (the geothermal ground) to the hot side of the TEMs. For that purpose, 2 m long will be inserted in the ground, since the temperature profile of the borehole where the generator will be installed shows that temperature does not significantly increase from 1.5 m deep, and 1 m will be out, since it is the part where TEMs would be located.

In order to determine if the TPCT was capable of transmitting the heat by means of phase change from the heat source to the modules, some experiments were performed. It was of interest to see if it reached an acceptable temperature distribution along different levels of the tube. Rope heaters were placed along 2 m of the TPCT to simulate the geothermal heat source and this part was insulated with rock wool. Fig. 2 represents the experimental assembly of these experiments. K-type thermocouples were placed in some levels of the TPCT as Fig. 2 shows, and temperature measurements were recorded. Tests were made

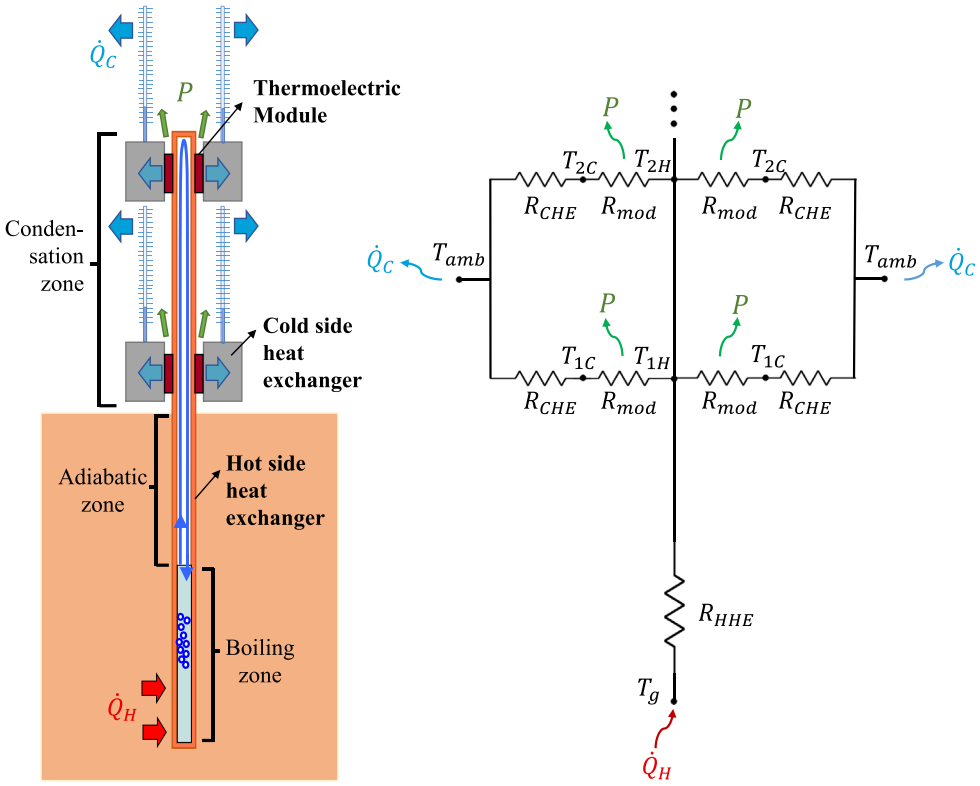

Fig. 1. Schematic of a Geothermal Thermoelectric Generator (GTEG).

Table 1
Heat fluxes and temperatures of the heat source for each test.

$\dot{Q}$ (W)	72.71	108.33	124.73	132.56	157.16
T_g (°C)	90.0	120.0	130.0	140.0	160.0

with the power source providing different heat fluxes ($\dot{Q}$) in order to obtain different temperatures representing conditions in the ground of the hot dry rock field in Timanfaya National Park. Values of heat flux and temperature are detailed in Table 1.

$$\dot{Q} = V_{source} I_{source} \tag{5}$$

The heat flux through the hot side heat exchanger was considered the provided by the source, as the insulation was enough to assume negligible losses. The thermal resistance R_{HHE} of the TPCT was calculated according to Eq. (2), where T_g is the temperature of the heat source simulating the ground, T_H was calculated as the average value of the 5 upper part levels and $\dot{Q}$ is the heat flux that goes through the TPCT from the lower part where the hot source is located to the upper part. This lead to the results represented in Figs. 3 and 4.

Fig. 3 shows that the temperatures' distribution along the hot side heat exchanger for different source temperatures has a decreasing tendency with height, reaching a maximum temperature decrease from the hot source to the 5th level of 14.6 °C.

According to these results, the upper part of the TPCT must hold the thermoelectric modules in the shortest possible length so that the temperature does not fall too much in the last levels.

As mentioned in the beginning of this section, low thermal resistances in the heat exchangers are important in order to maximize the power generation. It can be observed in Fig. 4 that this heat exchanger based on phase change follows the characteristic decrease of thermal resistance when the heat flux increases. The reason is that a higher heat flux produces higher temperatures at the TPCT, thus the boiling and condensation coefficients are improved and the associated thermal resistances reduced. Accordingly, the TPCT's thermal resistance diminishes from a value of 0.15 K/W when it transports 73 W to 0.07 K/W with 157 W.

This implies that if more thermoelectric modules and, thus, more cold side heat exchangers are added, it will make the heat flux increase, the thermal resistance decrease and that is translated into a higher power generation [25]. Besides that, as seen in Fig. 3, these thermoelectric modules should be compacted in the shortest length in order not to lose temperature with height. Otherwise, a decrease in the upper temperatures would produce a lower ΔT between the TEM's hot and cold sides inducing less efficiency per module and thus a lower total generated power. These results lead to the conclusion that compactness in the cold side heat exchangers is strongly needed to maximize power generation.

2.2. Cold side heat exchangers

The cold side heat exchanger consists of four 500 mm long sintered heat pipes with a diameter of 8 mm inserted horizontally and then inclined in a $70 \times 90\,mm^2$ fins dissipater with a base 14.5 mm thick and fifteen $40 \times 1.5\,mm^2$ corrugated fins. The TPCT's study indicated that it is desirable to install more TEMs, but that they do not take up much space in the tube in order not to lose efficiency in the modules. Although having the heat pipes vertically would permit a better return of the internal fluid, the configuration with horizontal heat pipes permits installing more heat exchangers per unit of length, since less separation is required, leading to more compactness. It is known that the inclination angle affects the performance of heat pipes [29]. In order to see if this configuration affects the CHE's performance, first its thermal resistance was obtained for different heat fluxes in completely vertical and then in horizontal position. The next step consisted in bending the heat pipes with the desired curvature and test again in the same way. Finally, commercial aluminum $104 \times 27.5 \times 0.3\,mm^3$ fins were added with a separation of 5 mm [30], trying to cover the longer length of the tubes as possible and it was characterized once again.

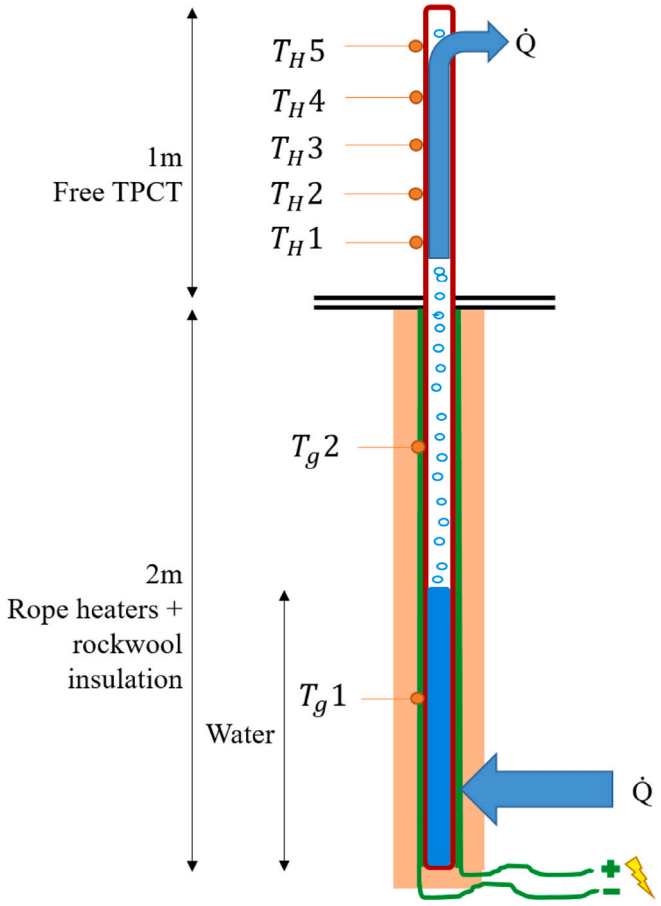

Fig. 2. Schematics of the Two Phase Closed Thermosiphon (TPCT) tests.

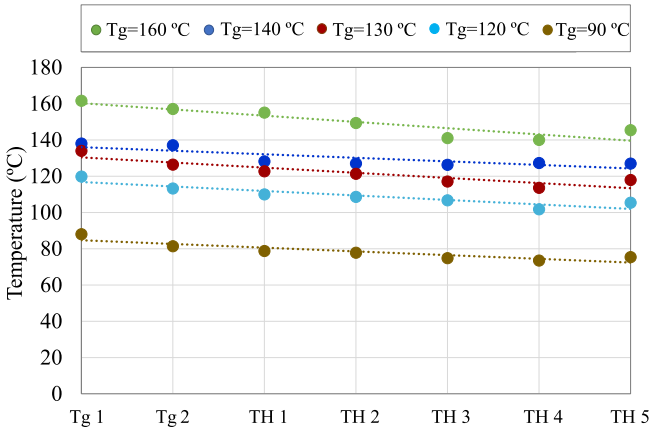

Fig. 3. Temperature distribution obtained in the TPCT tests.

The methodology followed to determine the thermal resistance of each case is summarized in the schematics of Fig. 5. Hence, cartridge heaters supplied the heat flux $\dot{Q}_C$ of each experiment by Joule effect. Rock wool insulation was added around these heaters so that heat flowed through the heat exchanger. The temperature at the base of the heat exchanger T_C and in the climatic chamber T_{amb} were measured, based on which the thermal resistance was calculated according to Eq. (3). In all the tests, the ambient temperature of the climatic chamber was 20 °C and the air velocity was 1 m/s.

Fig. 6 shows the results of the 4 configurations studied: in completely vertical position, completely horizontal, then with bent tubes

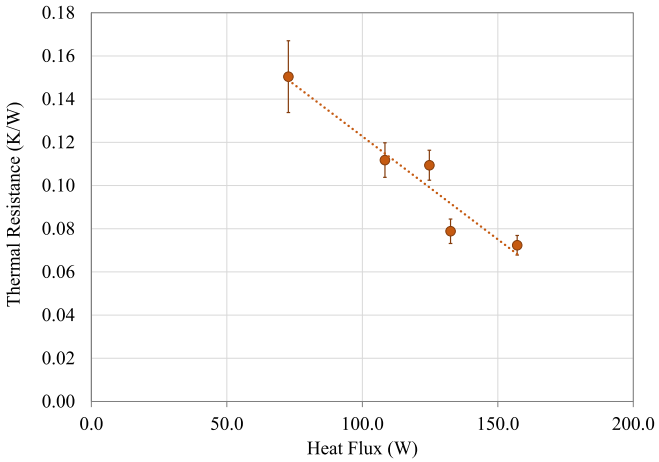

Fig. 4. Thermal Resistance of the TPCT. Uncertainties have been calculated according to [28].

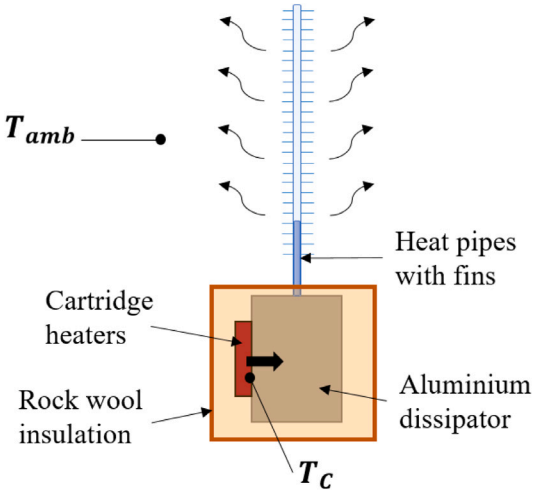

Fig. 5. Schematics of the test to determine the thermal resistance of the cold side heat exchangers.

and finally the working configuration, with bent tubes and fins. Here, the characteristic decrease of thermal resistance with increasing heat fluxes of phase change heat exchangers can be observed once again.

The horizontal configuration presents the highest thermal resistance, reaching 1.08 K/W for a 20 W heat flux. If the configuration is vertical, this thermal resistance decreases 12.8%. But if the thermal resistance in the vertical configuration is compared to the one with bent tubes, these are very similar, with an average value of 0.87 K/W in both cases. This means that there is no influence of the horizontal section of the tubes.

As the thermal resistance of the cold side heat exchanger with vertical heat pipes is nearly the same as with horizontal bent heat pipes, and this last shaping allows more compactness, it is confirmed that the chosen configuration is the most adequate for this GTEG.

The last test was in the configuration with bent tubes and fins. Here, the thermal resistance decreases 52.87% from the result with only bent tubes. The reason is that convection resistance is the most influential, and, according to heat transfer laws, fins reduce this resistance. The thermal resistance of the heat exchanger in this configuration, that was decided to be placed at the developed GTEG, varies between 0.42 K/W for a 20 W flux and 0.40 K/W for a 140 W flux.

Although these values are slightly higher than the ones obtained by simulation with loop thermosiphons by Catalan et al. which had

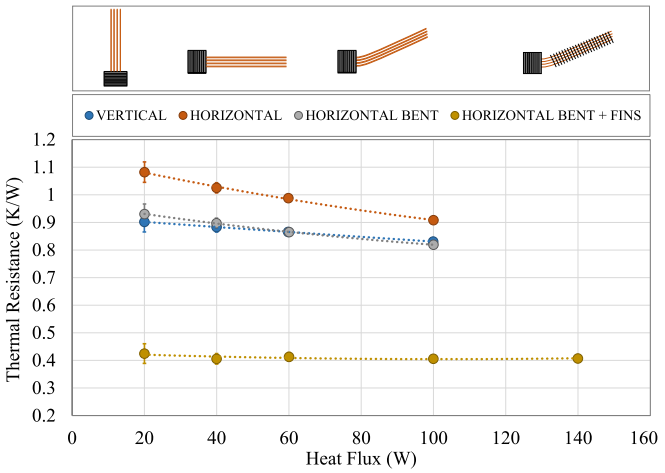

Fig. 6. Thermal resistance results of the Cold Side Heat Exchanger. Uncertainties have been calculated according to [28].

thermal resistances of between 0.16 - 0.20 K/W [25], the developed configuration is more compact, permitting the addition of more thermoelectric modules per unit of length of the hot side heat exchanger, leading to a minimum temperature drop, lower visual impact, and easing the assembly and field installation.

3. Prototype's description

Once proved that both the hot and cold side heat exchangers have low thermal resistance values and are appropriate for the geothermal thermoelectric generator, this section describes the whole GTEG.

According to Section 2.2, the thermal characterization of the two phase closed thermosiphon presents a decrease in the temperatures with an increase of the length. Hence, as more thermoelectric modules are added, the required length of the thermosiphon increases and therefore, the temperature difference between the sides of the upper thermoelectric modules will diminish. If this happens, their efficiency, i.e., their ability to convert heat into electrical energy through the Seebeck effect, would also diminish, reducing the generated power.

In order to check the theoretical results in practice, it was decided to build two geothermal thermoelectric generators with thermosiphons of different lengths. This will allow comparing the influence of the modules number and the temperature decrease with height. In these two hot side heat exchangers, the part inserted in the hot source is equal but the part with thermoelectric modules is 1 m long with 10 TEMs in one of them and 0.85 m with 6 modules in the other one. The modules are Marlow TG12-8L [31], composed by 127 Bismuth-Telluride thermocouples and able to operate with temperatures up to 230 °C, which were selected because of their adequacy for the temperature range in which the GTEG will work. In the generator, they are series-connected by pairs and these are placed one in front of each other, with one cold side heat exchanger per module (see Fig. 7).

As Fig. 8 shows, a copper block is responsible for transmitting the heat from the thermosiphon to the hot side of the module, adapting the round shape of the TPCT to the plane shape of the TEM. The cold side heat exchangers consist in the devices described at the beginning of Section 2.2. These are placed in the upper part of the thermosiphon, each 15 cm apart because this is the minimum distance that is allowed by the curvature of the heat pipes. This way, there are 5 levels in the bigger thermosiphon and 3 levels in the smaller one.

A graphite sheet is used as thermal interface material (TIM) between the copper block and the hot face of the module and between the cold face and the cold side heat exchanger. The whole cold side is assembled to the TPCT on the hot side. Therefore, contact will be a very critical point in the assembly, since the temperatures in the faces of the modules will depend on it [32].

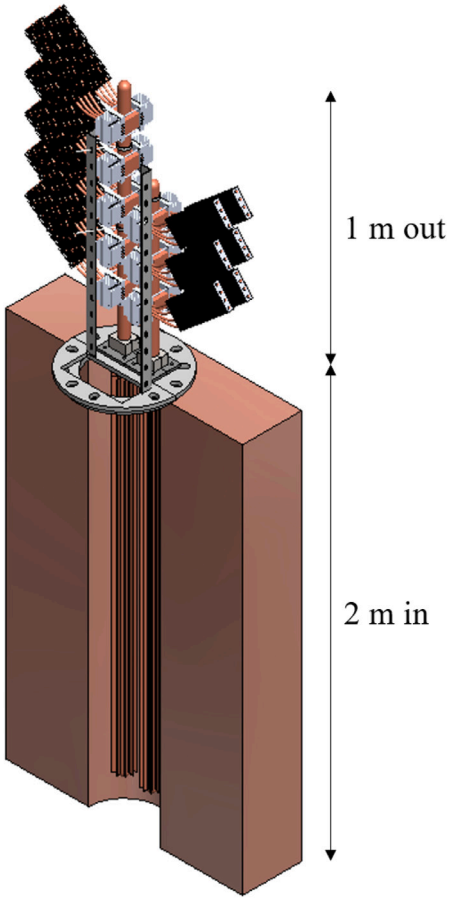

Fig. 7. Three-dimensional design of the GTEG.

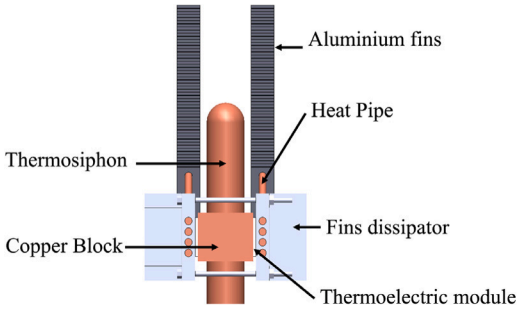

Fig. 8. Cold side assembly.

After checking the good performance of the heat exchangers, the whole devices were assembled. Fig. 9 depicts this assembly installed in a structure built at the laboratory simulating the borehole.

To resemble the geothermal heat at the laboratory, rope heaters were coiled around the inserted length of the two phase closed thermosiphon, and covered first with a 150 mm layer of rock wool (k = 0.035 W/mK) and afterward with a 20 mm layer of neoprene (k = 0.1 W/mK) to avoid thermal losses. The upper part of the hot side heat exchanger was also insulated with rock wool to ensure that condensation occurs only on the thermoelectric modules. An obus valve was welded to the two phase closed thermosiphon in order to fill it with a part of distilled water and to purge the interior air.

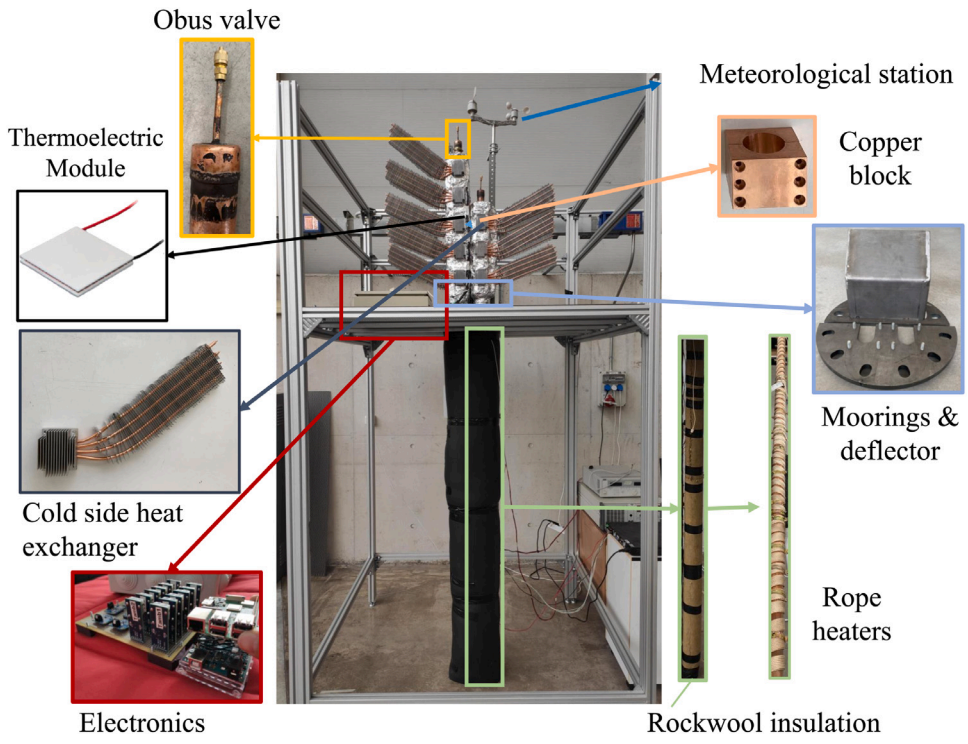

Fig. 9. Complete GTEG constructed in laboratory. Depiction of the main parts that compose it.

Table 2
Resolution and accuracy of the measuring instruments.

Instrument	Measure	Accuracy	Resolution
INA219 Sensor	Voltage (V)	±0.02	0.01
INA219 Sensor	Current (A)	±0.02	0.01
K-type thermocouple SRTC-GG-KI-2M	Temperature (°C)	±0.5	0.1
Anemometer Ahlborn FVAD15-H	Air velocity (m/s)	±1.5%	0.01

4. Results

This section presents and explains the obtained results of the whole geothermal thermoelectric generator's experimentation at the laboratory, focusing on the study of its generation capabilities for different operating conditions. In order to differentiate the two generators, from now on, the prototype with 10 thermoelectric modules is denoted Prototype A, while the 6 modules one, Prototype B.

Different sensors were installed in various positions (shown in Fig. 10) of the GTEG to carry out the study. Regarding the temperatures, in each prototype the external temperature of the tube was measured at the lower part, which simulates the geothermal heat source's temperature (T_g). Also, temperatures at the first and last levels of each prototype were measured in both faces of the thermoelectric module (T_H) for the hot side and (T_C) for the cold one. Additionally, temperatures in two points of the ambient (T_{amb1} and T_{amb2}) were monitored. There were also two temperature measurements at the external layer of the insulation neoprene (T_{los1}) and (T_{los2}) in order to confirm there were not thermal losses. All of them were measured by means of K-type thermocouples and Maxim Integrated MAX31855PMB1 peripheral modules [33]. Their corresponding resolution and accuracy data are detailed in Table 2.

In addition, there were 8 total measurement points of the generated power, one per pair of thermoelectric modules connected in series. This generation was obtained by sensing voltage (V) and current intensity (I) thanks to Adafruit INA219 breakout boards at each level [34]. These devices were connected to an Arduino plate which registered the data and sent it to a Raspberry Pi which was able to process the data and upload them to a server. This allowed monitoring remotely the performance of the GTEG.

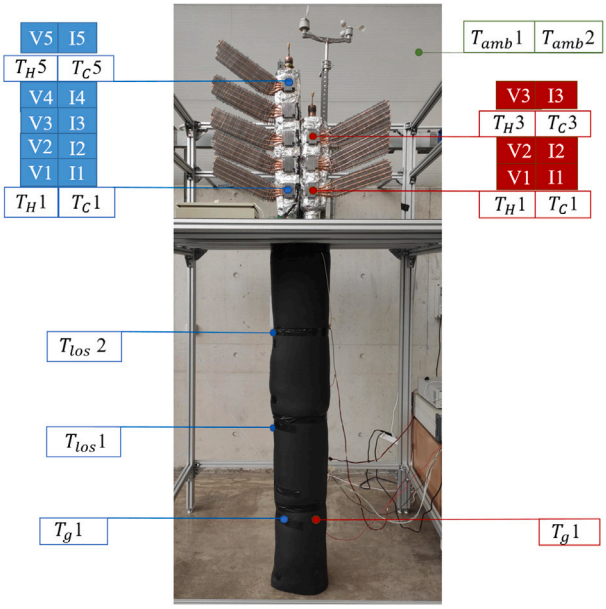

Fig. 10. Temperature, voltage and intensity measurement points.

4.1. Optimum load resistance

The first experiment's objective was to find out the optimum electrical load resistance (R_{Load}) that maximizes generation, as the modules' efficiency depends on the electrical loads to which they are connected. For that purpose, a heat flux was supplied to the rope heaters in order to maintain a constant source temperature of 120 °C. The modules in each level were connected to different electrical resistors of the following

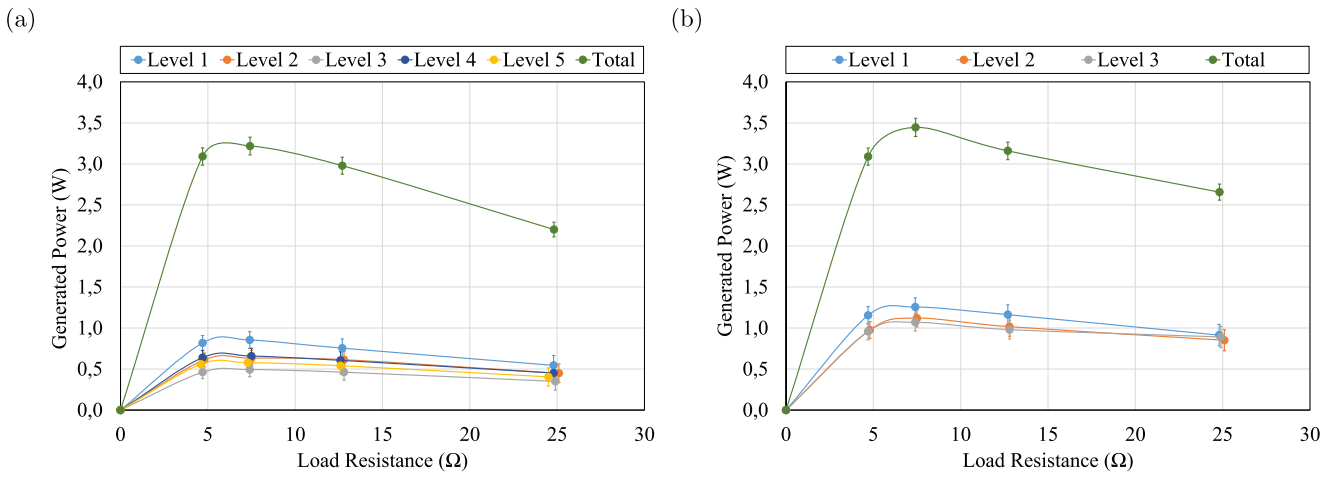

Fig. 11. Generated Power by GTEGs for different electrical load resistances. (a) Prototype A. 10 TEM, 5 levels. (b) Prototype B. 6 TEM, 3 levels.

values: open-circuit, 4, 6.6, 12 and 22.6 Ω and when the temperatures stabilized, the generated power for each load resistance was measured.

The results of this experiment for prototype A (10 modules) and B (6 modules) are represented in Fig. 11, where both prototypes reach the maximum generated power for 6.6 Ω, having a fast increase for low load resistances and after a slow decrease for higher values of load resistances. As in each level there are 2 modules in series, the optimum R_{Load} is 3.3 Ω per module, a very similar value to the one obtained in Catalan's article [25] and also to the internal electrical resistance of the modules [31]. Thus, the next experiments were made with the modules connected to this optimum load resistance.

4.2. Power generation

The following target was to test the operation of the prototype under different conditions to see if this generator is adequate to be installed in the mentioned shallow hot dry rock field.

The generator was working at the laboratory during 10 days in which the supplied power to the rope heaters was varied in order to get different temperature differences between the simulated ground and the environment. Tests were made first in natural convection and then in forced convection with a 1.5 m/s wind provided by a fan. These later tests resemble better to real conditions where forced convection is expected to be continuously present.

Fig. 12 shows the total generated power for different temperature differences between heat source and ambient for prototypes A and B. The maximum generated power by both prototypes was 36 W for a temperature difference of 160 °C, from which 17 W correspond to prototype A, and 19 W to prototype B.

Both GTEGs behave the same way, presenting a generated power that always linearly grows with the temperature difference between source and ambient. In both cases, for equal temperature difference between source and ambient, the generated power is higher in forced convection because wind improves the convection heat transfer coefficient (h) [35,36], reducing the cold side heat exchanger's thermal resistance, which brings its temperature closer to the ambient temperature, thus increasing the module's efficiency, which permits the modules to generate more power.

Also for both prototypes the slope of the tendency line is greater in forced convection. As the temperature difference between the hot and the cold sources increases, the difference between the generation with wind and without wind increases. This happens because in natural convection, there is a part of the heat dissipated by the lower levels that reaches the upper levels and does not allow the difference in temperature between the faces of the modules in the upper levels be as high as in the lower ones. When there is wind, it prevents the lower dissipaters' heat from reaching the top, homogenizing the boundary conditions. Therefore, a greater difference in temperature between sources makes the increase in generation more noticeable in the presence of wind.

The tendency of prototype B has a steeper slope than those of prototype A, and the generated power by B for the same thermal difference is greater than in A. As an example, when the temperature difference between source and ambient in forced convection is 150 °C, Prototype A generates 14.7 W while Prototype B generates 17.4 W.

Furthermore, for the same temperature difference, total generated power experiences a greater increase in the presence of wind in prototype B than in prototype A. For example, for a thermal difference of 140 °C, the power generated by prototype A in forced convection increases 50% with respect to natural, while in prototype B the increase is 82%. As in these GTEGs there is one CHE per thermoelectric module but all modules share the same HHE, considering the thermal resistance equivalent scheme of Fig. 1 there is a common hot side branch and as many parallel branches in the cold side as TEMs in the generator. Prototype A, which has 10 modules, has 10 parallel branches in the cold side and its equivalent thermal resistance will be lower than in Prototype B, that has only 6 modules. Then, as the equivalent cold side thermal resistance diminishes with more TEMs, the hot side thermal resistance becomes more significant. Since the wind reduces the CHE's thermal resistance (by increasing the convective heat transfer coefficient, h), this improvement is more noticeable in prototype B, because in prototype A the improvement is camouflaged by the predomination of the HHE's thermal resistance.

In order to see the generation difference in each level of the prototypes, these values are represented in Fig. 13. As can be observed, there is a greater dispersion in the tests with natural convection than in forced. As the tests are long, lasting approximately two days each, there is a variation in the external conditions that cannot be controlled (ambient temperature, convection, sunlight...) which in natural convection have an influence. But when we introduce the wind, as it is forced convection, the conditions that take place in the vicinity of the prototype are homogenized and the results become more stable.

In Fig. 13 it can be seen that in prototype B the generation of each level is very similar, even identical in forced convection and following a trend of higher generation in the first level and lower in the last one, due to the proximity to the heat source and to the temperature drop that the TPCT experiments with height. However, it can also be observed that in prototype A there is a great differentiation between levels, being the first level the one that generates more electrical power. In this case, it does not follow a logical tendency according to the proximity to the heat source, which might be caused by an unsuccessful contact in some modules of prototype A, which could be different in each floor due to the possible variations in the manual assembly.

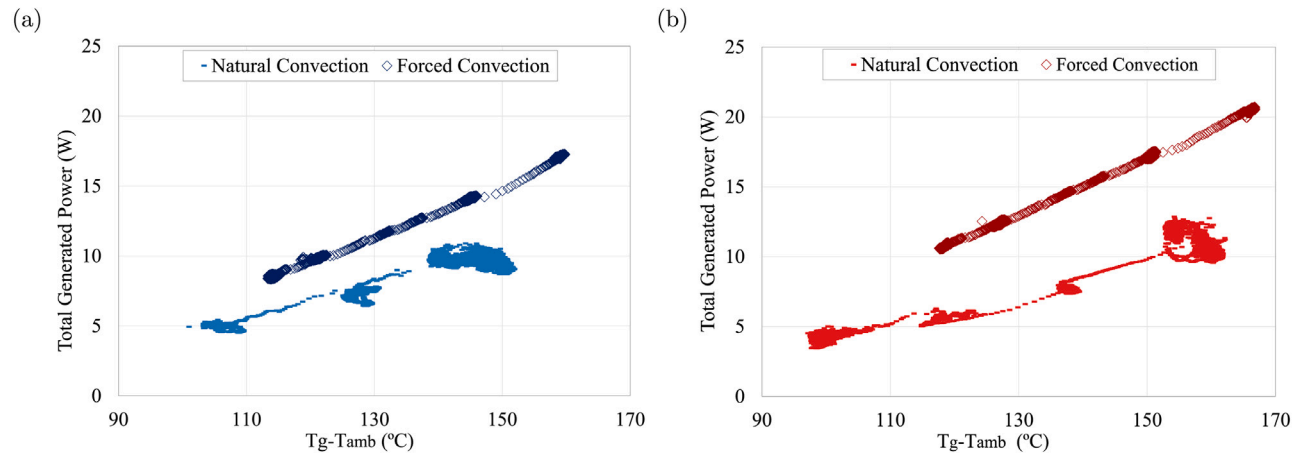

Fig. 12. Total Generated Power by GTEGs for different temperature difference between heat source and ambient. Comparison between natural and forced (v = 1.5 m/s) convection. (a) Prototype A. 10 TEM, 5 levels. (b) Prototype B. 6 TEM, 3 levels.

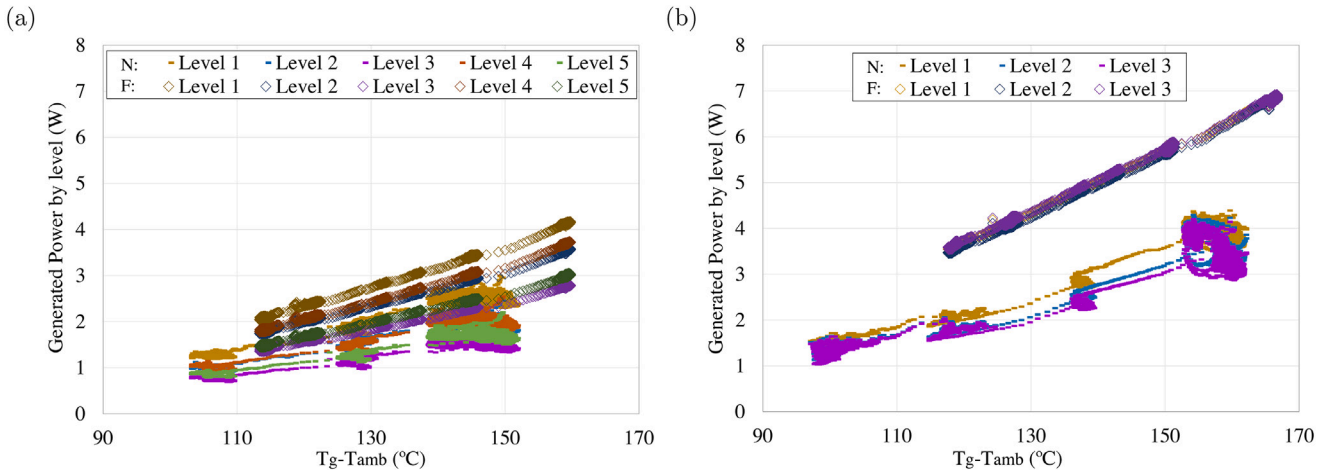

Fig. 13. Generated Power by GTEGs' level for different temperature difference between heat source and ambient. Comparison between natural and forced (v = 1.5 m/s) convection. (a) Prototype A. 10 TEM, 5 levels. (b) Prototype B. 6 TEM, 3 levels.

4.3. Thermal and efficiency analysis

To better understand the influence of convection on the thermal resistance of each part of the GTEG, the measured temperatures in different points were represented, both in natural and forced convection with a wind speed of 1.5 m/s, in a specific moment when the heat source and ambient temperatures were the same for both prototypes. These values are represented in Fig. 14. As can be observed, the main distinction is the thermal jump in the cold side heat exchanger, which is significantly lower in the presence of wind. Wind improves the convection coefficient and, according to Eq. (6), convective thermal resistance (R_{conv}) is inversely proportional to it. In the heat pipes' performance, boiling (R_b), condensation (R_c) and conduction (R_{cond}) resistances are also present in accordance with Eq. (7). Here, convection resistance is more significant than conductive and boiling thermal resistances [25,35,37] and therefore, an increase in h will produce that the total resistance of the heat pipe (R_{hp}) significantly decreases. Thus, the temperature in the cold side of the thermoelectric modules is very close to the ambient temperature. As a consequence, the temperature difference between the hot and cold sides of the thermoelectric modules is higher in forced than in natural convection. This effect is of interest, as the power generated by the modules depends on the thermal difference between their faces, and this GTEG is designed with the aim of a future installation in Timanfaya National Park (Spain), which is a windy zone. Values of ΔT_{HHE} and ΔT_{CHE} in Fig. 14 highlight the good performance of the developed heat exchangers, which obtain temperatures in the modules' sides close to the temperatures of the heat and cold sources, with the absence of auxiliary consumption, without moving parts nor need for maintenance.

$$R_{conv} = \frac{1}{hA\eta_{fins}} \tag{6}$$

$$R_{hp} = R_b + R_c + R_{cond} + R_{conv} \tag{7}$$

In view of the total generated power, forced convection is the most favorable case. As it is the expected condition in real operation, the GTEG's efficiency (η) was calculated in this condition in 3 cases of study for each prototype according to Eq. (8), where m is the number of thermoelectric modules per prototype, and $\dot{Q}$ is the heat provided by the source. The provided heat flux, average temperatures in both sides of the thermoelectric modules, total generated power and the efficiency values of each prototype are shown in Table 3.

$$\eta = \frac{\sum_{i=1}^{m} P_i}{\dot{Q}} = \frac{P_{tot}}{\dot{Q}} \tag{8}$$

$$\dot{Q} = V_{source} I_{source} \tag{9}$$

Fig. 15 shows the efficiency results versus the temperature difference between the heat source and the ambient, in the ranges that could be found in field, where for equal heat source temperatures, the

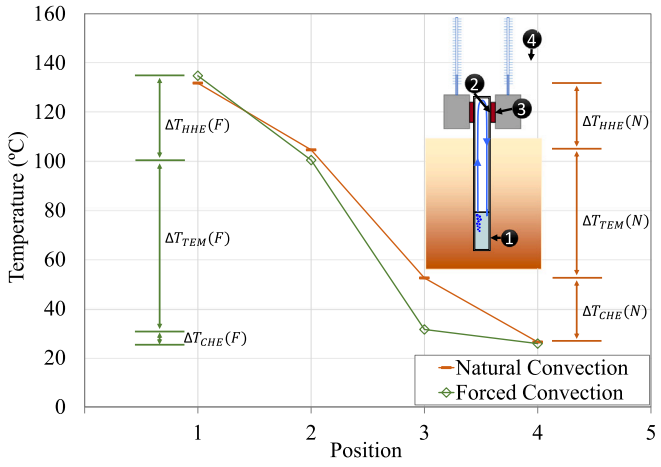

Fig. 14. Temperature drop in the Hot Side Heat Exchanger (HHE), Thermoelectric Modules (TEM) and Cold Side Heat Exchanger (CHE) of prototype A. Comparison between natural and forced (v = 1.5 m/s) convection in a specific case where the temperature difference between the heat source and the ambient was 108 °C.

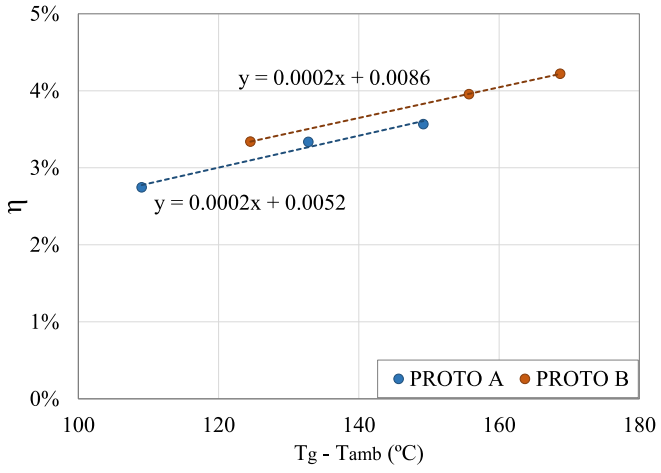

Fig. 15. Thermoelectric Modules' Efficiency vs. Thermal jump from the hot to the cold source. Comparison between Prototype A and B.

efficiency is 11% higher in prototype B than in A for a temperature difference between the heat source and the ambient of 130 °C and 10% higher for a difference of 150 °C, following a linear tendency. For a temperature difference between the heat source and the ambient of 160 °C, prototype B reaches an efficiency of 4.06% while prototype A, 3.72%, following the linear tendency. This decrease confirms that a higher length in the thermosiphon, despite having more thermoelectric modules, does not lead directly to major power generation, but instead have a negative influence, making the geothermal thermoelectric generator less efficient. This is in accordance with the thermal resistances equivalent scheme in Fig. 1, from which one can deduce that if we add thermoelectric modules, the equivalent hot side resistance per thermoelectric module ($R_{HHE} \cdot m$) is higher, and as a consequence, the hot side temperature of the module (T_H) diminishes, obtaining a lower ΔT and less efficiency in the module.

5. Conclusions

In conclusion, this article has demonstrated experimentally the feasibility of thermoelectricity to generate electricity from high enthalpy geothermal anomalies in shallow hot dry rock fields. The generator developed in this work is capable of generating 36 W in total (from

Table 3
Heat flux, hot and cold side temperatures average of the TEMs, total generated power and efficiency of each prototype (A and B), represented in 3 cases of study for each prototype with forced convection (v = 1.5 m/s).

Case	$\dot{Q}$ (W)	T_H (°C)	T_C (°C)	P_{tot} (W)	η (%)
A-1	332.67	100.4	31.5	9.14	2.75
A-2	425.10	118.3	31.3	14.18	3.34
A-3	470.55	128.4	33.7	16.78	3.57
B-1	343.96	121.0	33.9	11.49	3.34
B-2	439.39	143.0	34.4	17.38	3.96
B-3	482.72	156.9	37.8	20.38	4.22

which 17 W correspond to the power generated by prototype A, and 19 W by prototype B) with a temperature difference between the heat source and the environment of 160 °C, without auxiliary consumption.

By means of an experimental study of different heat exchangers, a GTEG was designed with a thermal resistance of 0.07 K/W in the hot side heat exchanger and 0.4 K/W in the cold side heat exchanger. Both exchangers are totally passive, as their operating principle is phase change. Furthermore, water is their working fluid, which makes them totally innocuous.

Different temperature and convection conditions were tested, demonstrating that this passive GTEG performs well in forced convection, with efficiency values (for a temperature difference between the heat source and the environment of 160 °C) of 4.06% in the prototype with 6 modules and 3.72% for the one with 10 modules, but which is able to operate even in natural convection.

The influence of height in the generator's efficiency was also determined, demonstrating that an increase in the number of thermoelectric modules in the GTEG may cause a drop in the total power generation. Moreover, the decrease in efficiency when the number of modules is increased, remarks the importance of compactness in these GTEGs.

This thermoelectric generator for geothermal energy (GTEG) is a novel and robust device without moving parts nor need for maintenance, which is able to use a constant, reliable and renewable source of energy with low impact. In short, a passive generator that demonstrates the viability of this technology to take advantage of the natural resources as high enthalpy geothermal anomalies present in shallow hot dry rock fields and to provide electricity in a renewable and environmentally friendly way.

Declaration of competing interest

The authors declare that they have no known competing financial interests or personal relationships that could have appeared to influence the work reported in this paper.

References

[1] P. to the United Nations Framework Convention on Climate Change, Paris agreement, 2016.
[2] K. Li, H. Bian, C. Liu, D. Zhang, Y. Yang, Comparison of geothermal with solar and wind power generation systems, Renew. Sustain. Energy Rev. 42 (2015) 1464–1474, http://dx.doi.org/10.1016/j.rser.2014.10.049.
[3] P. Olasolo, M.C. Juárez, M.P. Morales, S. Damico, I.A. Liarte, Enhanced geothermal systems (EGS): A review, Renew. Sustain. Energy Rev. 56 (2016) 133–144, http://dx.doi.org/10.1016/j.rser.2015.11.031.
[4] U.N.G. Aseembly, Transforming our world: the 2030 Agenda for Sustainable Development, 2015.
[5] T. Ahmad, F. Soelaiman, Electric renewable energy systems. Geothermal energy, Electr. Renew. Energy Syst. (2016) 114–139, http://dx.doi.org/10.1016/B978-0-12-804448-3/00007-4.
[6] A.T. Hoang, Waste heat recovery from diesel engines based on Organic Rankine Cycle, Appl. Energy 231 (2018) 138–166, http://dx.doi.org/10.1016/j.apenergy.2018.09.022.
[7] P. Valdimarsson, P. Valdimarsson, Geothermal power plant cycles and main components. URL https://www.researchgate.net/publication/266459027.

[8] D.W. Brown, D.V. Duchane, G. Heiken, V.T. Hriscu, Mining the Earth's Heat: Hot Dry Rock Geothermal Energy, Springer-Verlag Berlin Heidelberg, 2012, http://dx.doi.org/10.1007/978-3-540-68910-2, URL https://www.springer.com/gp/book/9783540673163.
[9] S. Ganguly, M.S.M. Kumar, Geothermal reservoirs-a brief review, J. Geol. Soc. India 79 (2012) 589–602.
[10] I.G.M. Español, Evaluación del Potencial Geotérmico Superficial de Montañas de Fuego como Sistema de Roca Caliente Seca [Tech. rep.], 1992.
[11] A.G. Camacho, J.F. Prieto, E. Ancochea, J. Fernández, Deep volcanic morphology below Lanzarote, Canaries, from gravity inversion: New results for Timanfaya and implications, J. Volcanol. Geotherm. Res. 369 (2019) 64–79, http://dx.doi.org/10.1016/j.jvolgeores.2018.11.013.
[12] D. Astrain, J.G. Vián, A. Martínez, A. Rodríguez, Study of the influence of heat exchangers' thermal resistances on a thermoelectric generation system, Energy 35 (2010) 602–610, http://dx.doi.org/10.1016/j.energy.2009.10.031.
[13] H.R. Takleh, V. Zare, Employing thermoelectric generator and booster compressor for performance improvement of a geothermal driven combined power and ejector-refrigeration cycle, Energy Convers. Manage. 186 (2019) 120–130, http://dx.doi.org/10.1016/j.enconman.2019.02.047.
[14] A.T. Hoang, X.P. Nguyen, A.T. Le, M.T. Pham, T.H. Hoang, A.R.M. Al-Tawaha, S. Yondri, Power generation characteristics of a thermoelectric modules-based power generator assisted by fishbone-shaped fins: Part II–Effects of cooling water parameters, Energy Sources A 43 (2021) 381–393, http://dx.doi.org/10.1080/15567036.2019.1624891.
[15] S. Khanmohammadi, M. Saadat-Targhi, F.W. Ahmed, M. Afrand, Potential of thermoelectric waste heat recovery in a combined geothermal, fuel cell and organic Rankine flash cycle (thermodynamic and economic evaluation), Int. J. Hydrogen Energy 45 (2020) 6934–6948, http://dx.doi.org/10.1016/j.ijhydene.2019.12.113.
[16] E. Gholamian, A. Habibollahzade, V. Zare, Development and multi-objective optimization of geothermal-based organic Rankine cycle integrated with thermoelectric generator and proton exchange membrane electrolyzer for power and hydrogen production, Energy Convers. Manage. 174 (2018) 112–125, http://dx.doi.org/10.1016/j.enconman.2018.08.027.
[17] M.Z. Malik, F. Musharavati, S. Khanmohammadi, A.H. Pakseresht, S. Khanmohammadi, D.D. Nguyen, Design and comparative exergy and exergo-economic analyses of a novel integrated Kalina cycle improved with fuel cell and thermoelectric module, Energy Convers. Manage. 220 (2020) http://dx.doi.org/10.1016/j.enconman.2020.113081.
[18] C. Suter, Z.R. Jovanovic, A. Steinfeld, A 1kWe thermoelectric stack for geothermal power generation - Modeling and geometrical optimization, Appl. Energy 99 (2012) 379–385, http://dx.doi.org/10.1016/j.apenergy.2012.05.033.
[19] C. Liu, P. Chen, K. Li, A 500 W low-temperature thermoelectric generator: Design and experimental study, Int. J. Hydrogen Energy 39 (2014) 15497–15505, http://dx.doi.org/10.1016/j.ijhydene.2014.07.163.
[20] C. Liu, P. Chen, K. Li, A 1 KW thermoelectric generator for low-temperature geothermal resources.
[21] K. Li, G. Garrison, M. Moore, Y. Zhu, C. Liu, R. Horne, S. Petty, An expandable thermoelectric power generator and the experimental studies on power output, Int. J. Heat Mass Transfer 160 (2020) http://dx.doi.org/10.1016/j.ijheatmasstransfer.2020.120205.
[22] K. Wang, X. Wu, Downhole thermoelectric generation in unconventional horizontal wells, Fuel 254 (2019) http://dx.doi.org/10.1016/j.fuel.2019.05.113.
[23] R. Dell, C.S. Wei, M.T. Petralia, G. Gislason, R. Unnthorsson, Thermoelectric powered security systems in iceland using a geothermal steam pipe as a heat source, Proceedings 2 (2018) 440, http://dx.doi.org/10.3390/icem18-05309.
[24] R. Ahiska, H. Mamur, Design and implementation of a new portable thermoelectric generator for low geothermal temperatures, IET Renew. Power Gener. 7 (2013) 700–706, http://dx.doi.org/10.1049/iet-rpg.2012.0320.
[25] L. Catalan, M. Araiz, P. Aranguren, D. Astrain, Computational study of geothermal thermoelectric generators with phase change heat exchangers, Energy Convers. Manage. 221 (2020) http://dx.doi.org/10.1016/j.enconman.2020.113120.
[26] J. Carracedo, E.R. Badiola, V. Soler, Aspectos volcanológicos y estructurales, evolución petrológica e implicaciones en riesgo volcánico de la erupción de 1730 en Lanzarote, Islas Canarias. URL http://estudiosgeol.revistas.csic.es/index.php/estudiosgeol/article/view/436/456.
[27] I.G.y Minero de España (IGME), M. de Industria y Energía, S. de la Energía y Recursos Minerales, Análisis y valoración de las técnicas geofísicas aplicadas a la investigación geotérmica, 1985, http://info.igme.es/SidPDF/035000/001/Analisis%20y%20valoracion%20de%20las%20tecnicas%20geofisicas%20apliacadas%20a%20la%20investigacion%20geotermica/35001_0002.pdf.
[28] H. Coleman, W. Steele, Experimentation, Validation and Uncertainty. Analysis for Engineers, third ed., Hoboken, NJ, USA, 2018,
[29] A.A. Alammar, R.K. Al-Dadah, S.M. Mahmoud, Effect of inclination angle and fill ratio on geyser boiling phenomena in a two-phase closed thermosiphon – Experimental investigation, Energy Convers. Manage. 156 (2018) 150–166, http://dx.doi.org/10.1016/j.enconman.2017.11.003.
[30] A. Casi, M. Araiz, L. Catalán, D. Astrain, Thermoelectric heat recovery in a real industry: From laboratory optimization to reality, Appl. Therm. Eng. (2020) http://dx.doi.org/10.1016/j.applthermaleng.2020.116275.
[31] M. INDUSTRIES, Technical data sheet for TG12-8 single-stage thermoelectric generator. URL https://cdn2.hubspot.net/hubfs/547732/Data_Sheets/TG12-8.pdf.
[32] A. Rodríguez, G. Pérez-Artieda, I. Beisti, D. Astrain, A. Martínez, Influence of temperature and aging on the thermal contact resistance in thermoelectric devices, J. Electron. Mater. (2020) http://dx.doi.org/10.1007/s11664-020-08015-y.
[33] MAX31855PMB1 peripheral module general description. URL www.maxim-ic.com.
[34] Adafruit INA219 current sensor breakout. URL https://learn.adafruit.com/adafruit-ina219-current-sensor-breakout.
[35] A. Bejan, A.D. Kraus, Heat Transfer Handbook, J. Wiley, 2003, p. 1480.
[36] R. Mazón-Hernández, J.R. García-Cascales, F. Vera-García, A.S. Káiser, B. Zamora, Improving the electrical parameters of a photovoltaic panel by means of an induced or forced air stream, Int. J. Photoenergy 2013 (2013) http://dx.doi.org/10.1155/2013/830968.
[37] H.K. Forster, N. Zuber, Dynamics of vapor bubbles and boiling heat transfer, A.I.Ch.E. J. (1955) URL https://doi.org/10.1002/aic.690010425.